Blocking Effect and Crystal Structure of Natrin Toxin, a Cysteine-Rich Secretory Protein from *Naja atra* Venom that Targets the BK_{Ca} Channel[†,‡]

Jing Wang,[§,||] Bing Shen,[§,||] Min Guo,[§,||] Xiaohua Lou,[§,||] Yuanyuan Duan,[§] Xin Ping Cheng,[§] Maikun Teng,*[,§,||] Liwen Niu,*[,§,||] Qun Liu,[⊥] Qingqiu Huang,[⊥] and Quan Hao[⊥]

Hefei National Laboratory for Physical Sciences at Microscale and School of Life Sciences, University of Science and Technology of China, Hefei, Anhui 230027, China, Key Laboratory of Structural Biology, Chinese Academy of Sciences, and MacCHESS, Cornell High Energy Synchrotron Source, Cornell University, Ithaca, New York 14853

Received April 3, 2005; Revised Manuscript Received June 6, 2005

ABSTRACT: Cysteine-rich secretory proteins (CRISPs) are widespread in snake venoms. Some members of these CRISPs recently have been found to block L-type Ca^{2+} channels or cyclic nucleotide-gated ion (CNG) channels. Here, natrin purified from *Naja atra* venom, a member of the CRISP family, can induce a further contractile response in the endothelium-denuded thoracic aorta of mouse which has been contracted by a high-K^+ solution. Further experiments show it can block the high-conductance calcium-activated potassium (BK_{Ca}) channel in a concentration-dependent manner with an IC_{50} of 34.4 nM and a Hill coefficient of 1.02, which suggests that only a single natrin molecule is required to bind an ion channel to block BK_{Ca} current. The crystal structure of natrin displaying two domains in tandem shows its cysteine-rich domain (CRD) has relatively independent flexibility, especially for the C-terminal long loop (loop I) of CRD to participate in the interface of two domains. On the basis of previous studies of CNG channel and L-Ca^{2+} channel blockers, and the sequence and structural comparison of natrin and stecrisp, the deviation of the vital loop I of CRD is suggested to contribute to different effects of some CRISPs in protein−protein interaction.

Potassium channels (K^+ channels) are present widely in both excitable and nonexcitable cells and take part in many critical physiological processes, such as regulating neurotransmitter release, heart rate, insulin secretion, neuronal excitability, epithelial electrolyte transport, and smooth muscle contraction (*1*−*3*). The calcium-activated potassium (K_{Ca}) channel superfamily is a diverse class of K^+ channels, characterized by their dependence on the intracellular concentration of Ca^{2+} ions ($[Ca^{2+}]_i$).[1] According to their different single-channel conductance, pharmacological, and voltage sensitivities, this superfamily has been further subdivided into three distinct categories: high-conductance (100−250 pS, BK_{Ca}), intermediate-conductance (20−80 pS, IK_{Ca}), and low-conductance (5−20 pS, SK_{Ca}) calcium-activated K^+ channels (*4*). BK_{Ca} channels, which are of particular interest because of their large channel conductance and their expression in a range of excitable cell types, e.g., smooth muscle cells, can be activated by local Ca^{2+} transients (Ca^{2+} sparks) that are released through ryanodine receptors in the sarcoplasmic reticulum (*5*, *6*). Physiological activation of vascular BK_{Ca} channels may be an important buffering mechanism for counteracting vessel depolarization and constriction in response to some vasoconstrictors and to increased intravascular pressure (*7*, *8*). Because of their central role in regulating cell activity, modulation of BK_{Ca} channels is potentially useful for the treatment of a variety of disease states associated with both the central nervous system and smooth muscle function.

α-Subunits of BK_{Ca} channel construct the functional K^+-conducting pore, as a homotetramer (*9*). Its N-terminal region is a pattern of six transmembrane segments (segments S1−S6) with a pore region between S5 and S6. The C-terminal portion of this pore region forms the ion selectivity filter of K^+ channels as identified in the crystal structure of KcsA, a small bacterial K^+ channel protein (*10*, *11*). In a manner different from that of Kv channels, however, a large C-terminal domain (∼800 residues) plays a role in calcium sensing and acts as a partner for protein−protein interactions. In recent years, many peptides, including charybdotoxin (ChTX), kaliotoxin, and BmBKTx1, isolated from scorpion venoms, have been identified to be potent inhibitors of BK_{Ca} channels, blocking the passage of K^+ ions by binding at the

[†] This work is supported by research grants from the National Natural Science Foundation of China (Grants 30130080, 30025012, and 30121001), the 863 Plan ahd the 973 Plan of the Ministry of Science and Technology of China (Grants 2002BA711A13, G19999075603, and 2004CB520801), and the Chinese Academy of Sciences (Grants KSCX1-SW-17, STZ98-2-12, and STZ-01-29).

[‡] The atomic coordinates have been deposited in the RCSB Protein Data Bank as entry 1XX5.

* To whom correspondence should be addressed: Department of Molecular and Cell Biology, School of Life Sciences, University of Science and Technology of China, 96 Jinzhai Rd., Hefei, Anhui 230026, The People's Republic of China. Telephone: 86-551-3606334. Fax: 86-551-3603046. E-mail: lwniu@ustc.edu.cn and mkteng@ustc.edu.cn.

[§] University of Science and Technology of China.

[||] Chinese Academy of Sciences.

[⊥] Cornell University.

[1] Abbreviations: BK_{Ca}, high-conductance calcium-activated potassium; CRISP, cysteine-rich secretory protein; PR-1, pathogenesis-related proteins of group 1; CRD, cysteine-rich domain; CNG, cyclic nucleotide-gated; $[Ca^{2+}]_i$, intracellular concentration of Ca^{2+} ions; rmsd, root-mean-square deviation; PDB, Protein Data Bank; VSMC, vascular smooth muscle cell.

10.1021/bi050614m CCC: $30.25
Published on Web 07/07/2005

pore entryway on the extracellular side of the channel (*12*−*15*).

We have previously identified a 25 kDa toxin protein, natrin, purified from *Naja atra* venom, as a member of the cysteine-rich secretory protein (CRISP) family (*16*). CRISPs in the vertebrates are characterized by the 16 strictly conserved cysteines that form eight disulfide bonds and show apparent homogeneity with 35−85% sequence identity. Recently, in snake venoms, blocking effects on ion channels have also been found; pseudechetoxin (PsTx) from *Pseudechis australis* and pseudecin from *Pseudechis porphyriacus* can block cyclic nucleotide-gated ion (CNG) channels, and some venom toxins, for example, ablomin from *Agkistrodon blomhoffi*, can inhibit the contraction of smooth muscle (*17*−*19*). In another kind of reptile venom, helothermine (HLTx) from Mexican beaded lizard has been reported to alter the voltage-gated calcium channel and voltage-gated potassium channel (*20*, *21*). To elucidate the structural basis of the functions in CRISPs, the structure of stecrisp from *Trimeresurus stejnegeri* venom has been reported (*22*). Its crystal structure is separated into three regions, an N-terminal pathogenesis-related protein of the group 1 (PR-1) domain, a C-terminal cysteine-rich domain (CRD), and a hinge region linking the two motifs. Interestingly, CRD is structurally similar with two K^+ channel blockers, ShK from *Stichodacryla helianthus* and BgK from *Bunodosoma granulifera*, suggesting this domain may be related to the interaction with ion channels (*23*, *24*). But so far, whether stecrisp can act on K^+ channels has yet to be reported.

The results of this paper show that natrin also has a blocking effect, however, on the BK_{Ca} channel, a new type of ion channel apart from those influenced by its homologues. The interdomain motion first is observed in natrin crystal with relatively independent flexibility of CRD. A vital segment described in the studies of CNG channel and L-type Ca^{2+} channel blockers in CRISPs lies in loop I of CRD in the structural model of natrin and stecrisp. This loop participates in the interface of two domains and is flexible for modulating the interdomain motion. By alignment, this flexible loop is also a prominent variable in the primary sequences of CRISPs and displays more deviation, which implies it may play a vital role in some protein−protein interactions as a potentially functional site.

MATERIALS AND METHODS

Drugs. Charybdotoxin (ChTX), 4-aminopyridine (4-AP), type IA collagenase, papain, albumin bovine V, aspartic acid, Na_2ATP, *N*-(2-hydroxyethyl)piperazine-*N*′-2-ethanesulfonic acid (HEPES), and ethylene glycol bis(2-aminoethyl)-*N*,*N*,*N*′,*N*′-tetraacetic acid (EGTA) (Sigma Chemical Co., St. Louis, MO) and 1,4-dithiothreitol (DTT) (Promega, St. Louis, MO) were dissolved in a bath solution or a Ca^{2+}-free physiological salt solution (PSS). All concentrations are the final molar concentrations in the organ chambers.

Natrin Preparation. Natrin was purified as described previously (*16*). The purity of the protein was identified by mass spectrometry and SDS−PAGE. After being dissolved in the external solution, the protein was perfused in the bath at concentrations ranging between 1 nM and 1 μM.

Isolated Thoracic Aortic Strip Segment and Tension Measurement. The isolated thoracic aortic strip segment and tension measurement were the same as those described previously (*25*). Briefly, male white mice were anesthetized with an intraperitoneal injection of sodium pentobarbital (150 mg/kg) together with sodium heparin (100 IU/kg, ip) to prevent intravascular coagulation. At room temperature (22−25 °C), thoracic aorta of mouse was quickly dissected free and placed in Krebs Henseleit solution containing 118 mM NaCl, 4.7 mM KCl, 2.5 mM $CaCl_2$, 1.2 mM KH_2PO_4, 1.2 mM $MgSO_4{\cdot}7H_2O$, 25.2 mM $NaHCO_3$, and 11.1 mM glucose (pH 7.4 with NaOH). With a dissecting microscope, adhering perivascular tissue was carefully removed, and the descending thoracic aorta was cut into 2 mm long rings. The endothelium was removed with a wooden stick. The vessels were mounted onto two thin stainless steel holders in 2 mL organ baths containing Krebs Henseleit solution at 37 °C, and continuously bubbled with a gas mixture of 95% O_2 and 5% CO_2 to maintain a pH of 7.4. A movable device allowed the application of a passive tension of 500−550 mg, which was determined to be the optimal resting tension for obtaining the maximal active tension induced by a 60 mM K^+ solution containing 58 mM NaCl, 64.7 mM KCl, 2.5 mM $CaCl_2$, 1.2 mM KH_2PO_4, 1.2 mM $MgSO_4{\cdot}7H_2O$, 25.2 mM $NaHCO_3$, and 11.1 mM glucose (pH 7.4 with NaOH). The isometric tension was recorded on a polygraph (Biolap 420). After an equilibration period of 1 h, the contractile function of vessel was tested twice by replacing the Krebs Henseleit solution with a 60 mM K^+ solution. After washout, the vessels were treated with 1 μM natrin or contracted with a 60 mM K^+ solution again.

Cell Isolation, Electrophysiological Measurements, and Data Analysis. The thoracic aortic segments obtained as described above were placed in an ice-cold Ca^{2+}-free physiological salt solution (PSS) containing 55 mM NaCl, 80 mM sodium glutamate, 5.6 mM KCl, 10 mM HEPES, 2 mM $MgCl_2$, and 10 mM glucose (pH 7.4 adjusted with NaOH) and washed twice. With a dissecting microscope, adhering perivascular tissue was carefully removed and the vessel was opened longitudinally. The smooth muscle layer was obtained by tearing out adherent adventitia. Then this tissue was cut into small fragments, and incubated in plastic tube with 1 mL of Ca^{2+}-free PSS containing 20 mg/mL type IA collagenase, 0.5 mg/mL papain, 10 mg/mL albumin bovine V, and 1.75 mg/mL DTT at 37 °C for 36−39 min. After digestion, tissue masses were transferred to another plastic tube containing Ca^{2+}-free PSS with a wide-pore Pasteur pipet, and washed twice in this solution for 10 min each. Then, VSMCs were dispersed by gentle trituration with a slender Pasteur pipet; the cell suspension was transferred to the cell chamber, and well-attached VSMCs were selected for experiments.

Whole-cell currents were recorded by using an Axopatch 200B patch clamp amplifier (Axon Instruments, Foster City, CA) in voltage-clamp mode, controlled by the Igor Pro software package (WaveMetrics, Lake Oswego, OR). Patch pipets (resistance of 3−5 MΩ) were filled with an internal pipet solution containing 140 mmol/L KCl, 1 mmol/L $MgCl_2$, 10 mmol/L HEPES, 5 mmol/L EGTA, and 5 mmol/L Na_2-ATP (pH 7.2 with KOH). Micropipets were obtained from the Shanghai Brain Research Institute of the Chinese Academy of Sciences, and pulled with a micropipet puller (P-97, Sutter Instruments, Novato, CA). After gigaohm seals were obtained, the membrane was ruptured with a 5 ms pulse

to 1.3 VDC. Series resistance was typically compensated by 70%. The cells were held at −60 mV, and voltage steps ranging from −60 to 60 mV were applied for 200 ms in 10 mV step increments. All macroscopic currents were sampled at 50 kHz and filtered at 5 kHz, and data were analyzed with Igor Pro. Whole-cell current was normalized to cell capacitance and was expressed as picoamperes per picofarad (pA/pF). Changes in the BK_{Ca} current were detected in the absence and presence of natrin or ChTX. The bath solution contained 140 mM NaCl, 5.4 mM KCl, 1.8 mM $CaCl_2$, 1 mM $MgCl_2$, 0.1 mM $CdCl_2$, 10 mM Na-HEPES, 10 mM glucose, and 1 mM 4-AP (pH 7.2 with NaOH), and all experiments were performed at room temperature (22−25 °C). The bath chamber (2.5 mL) was superfused with a drug-containing or natrin toxin-containing solution at a rate of 4 mL/min. In natrin concentration−response experiments, every concentration (1 nM, 10 nM, 100 nM, and 1 μM) was repeated in 3−10 different cells.

Results of data analysis were expressed as means ± the standard error. The paired Student's *t*-tests were used to compare results in treated and untreated cells. Differences are considered to be significant when $P < 0.05$. In electrophysiological experiments, *n* represents the number of cells.

Crystallization, Data Collection, and Processing. Natrin was purified from *N. atra* venom, and crystal growth, data collection, and data processing were as previously described (*16*). The crystals belong to space group $P2_12_12_1$ with the following cell dimensions: $a = 101.68$ Å, $b = 90.75$ Å, and $c = 91.55$ Å.

Model Building and Refinement. The crystal structure of natrin was determined by molecular replacement using AMoRe (*26*). The solution of a trimer in an asymmetric unit was found with a correlation coefficient (CC) of 43.4 and an *R*-factor of 42.9% for data between 15.0 and 3.5 Å using PDB entry 1RC9 (*22*). At the beginning of the refinement, residues with unclear side chain electron density were mutated to alanines and water molecules were not included in the model. The refinement was initially carried out in a resolution range of 15−3.5 Å using the rigid body refinement in CNS (*27*). The model was examined and corrected manually by inspection of $2F_o - F_c$ and $F_o - F_c$ electron density maps using O (*28*). The model was then refined by simulated annealing and conjugate gradient methods, followed by temperature factor refinement. When the *R*-factor reached ∼25%, water molecules were added to the model according to the electron density maps, cycled with further refinements. The final model exhibited a crystallographic *R*-factor of 20.6% for all data with a 2σ cutoff in the resolution range of 8.0−2.4 Å, excluding the 5% randomly distributed reflections used to calculate the free *R*-factor, which dropped to a final value of 23.5%. The overall assessment of model quality was performed using PROCHECK (*29*), and the atomic coordinates have been deposited in the Protein Data Bank as entry 1XX5.

RESULTS

Effects of Natrin on Mouse Thoracic Aortic Contraction. We examined the effects of natrin on endothelium-denuded mouse thoracic aortic rings. Natrin (1 μM), the 25 kDa protein purified from *N. atra* venom, did not affect the basal tension of the denuded thoracic aortic rings in normal Krebs Henseleit solution ($n = 5$ rings from 5 mice; Figure 1A), but in another group, after the denuded thoracic aortic rings had been contracted with a 60 mM K^+ solution for ∼15 min, 1 μM natrin added to the organ bath induced a further contractile response and the percent response to 60 mM K^+ solution-induced contraction was 23.8 ± 1.6% ($n = 15$ rings from 10 mice; Figure 1B). On the other hand, some other rings were first contracted with a 60 mM K^+ solution. After repeated washing and another equilibration with Krebs Henseleit solution in these rings for 30 min, the rings were treated with 1 μM natrin for ∼10 min, and then contracted with a 60 mM K^+ solution with 1 μM natrin again (Figure 1C). The contractile force was significantly stronger in natrin-treated rings than that in the rings only contracted with a 60 mM K^+ solution (378 ± 24 mg vs 310 ± 23 mg, $n = 8$ rings from 4 mice, $P < 0.01$; Figure 1C), and the percent was 23.1 ± 2.3%. This percent was very consistent with the result of the contractile response induced by natrin after the rings were contracted with a 60 mM K^+ solution for ∼15 min.

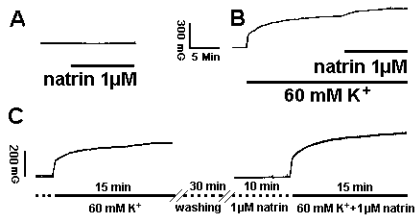

FIGURE 1: Natrin specifically inhibited high-K^+ solution-induced contraction in isolated thoracic aorta. (A) Natrin (1 μM) was added to the bath and could not affect the basal tension of the isolated thoracic aortic rings ($n = 5$ rings from 5 mice). (B) After the rings were exposed to a 60 mM K^+ solution for ∼15 min, 1 μM natrin could induce a further contraction. The percent response to a 60 mM K^+ solution was 23.8 ± 1.6% ($n = 15$ rings from 10 mice). (C) The rings were pretreated with 1 μM natrin for ∼10 min and then contracted with a 60 mM K^+ solution for ∼15 min. The contractile response treated by natrin was significantly higher than the untreated response (378 ± 24 mg vs 310 ± 23 mg, $n = 8$ rings from 4 mice, $P < 0.01$). The percent response of treated rings to untreated rings was 23.1 ± 2.3%.

Effect of Natrin on BK_{Ca} Currents in Mouse Vascular Smooth Muscle Cells. In the whole-cell voltage clamp experiment, natrin was found to inhibit BK_{Ca} currents in the isolated mouse vascular smooth muscle cells. Voltage-dependent macroscopic outward currents were recorded with a holding potential of −60 mV and an external solution containing 0.1 mM $CdCl_2$ which blocks Ca^{2+} currents completely, and the BK_{Ca} currents were isolated by adding 1 mM 4-AP to inhibit voltage-gated potassium channels in a bath solution. Furthermore, this kind of BK_{Ca} current was also identified by some BK_{Ca} channel blockers, TEA and ChTX according to published methods (*30*, *31*). TEA (1 mM), an inhibitor of BK_{Ca} channels, significantly suppressed the BK_{Ca} currents (from 1009 ± 134 to 341 ± 20 pA, at 60 mV, $n = 6$ cells, $P < 0.05$; Figure 2A). Similar results were also observed with 100 nM ChTX, a synthetic peptide toxin that more selectively blocks BK_{Ca} channels (from 973 ± 142 to 291 ± 36 pA, at 60 mV, $n = 3$ cells, $P < 0.05$; Figure 2A). As in BK_{Ca} channel antagonists, externally applying 100 nM natrin strikingly reduced BK_{Ca} currents evoked by a depolarizing pulse from −60 to 60 mV with a −60 mV holding potential (from 951 ± 150 to 373 ± 53 pA, at 60 mV, $n = 4$ cells, $P < 0.05$; Figure 2B).

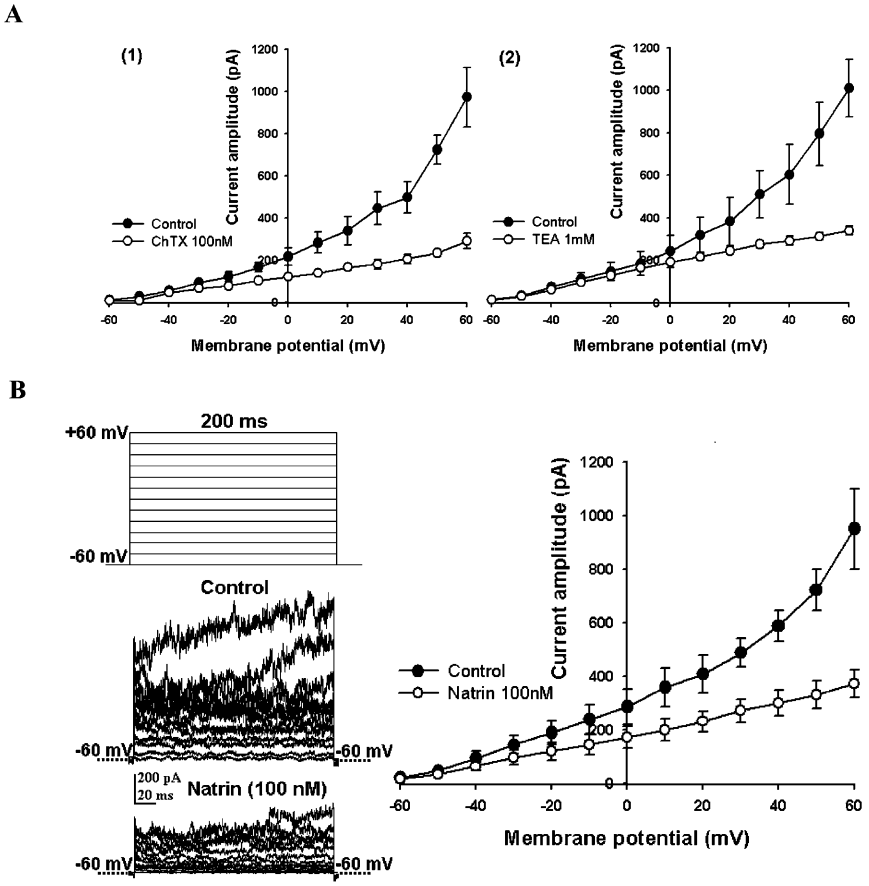

FIGURE 2: Effects of ChTX, TEA, and natrin on BK_{Ca} currents in vascular smooth muscle cells of mouse. (A) Current−voltage relationship ($I-V$) recorded at 60 mV with a −60 mV holding potential in the presence of 100 nM ChTX (1) ($n = 3$ cells) and 1 mM TEA (2) ($n = 6$ cells). (B) Current traces and current−voltage relationship ($I-V$) recorded at 60 mV with a −60 mV holding potential in the presence of 100 nM natrin ($n = 4$ cells).

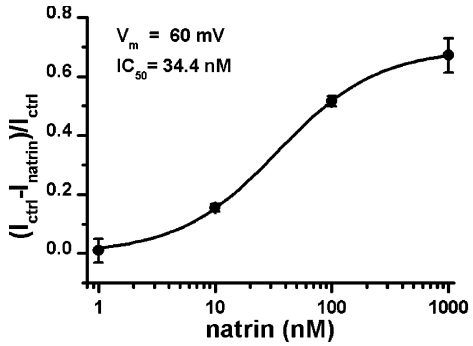

FIGURE 3: Concentration−response curve for the blockade of current (I) by natrin toxin. Experimental points were obtained at 60 mV with a −60 mV holding potential. The data were best fitted according to the logistic equation $(I_{control} - I_{natrin})/I_{control} = Block_{max}\text{-}[C^n/(C^n + IC_{50}{}^n)]$, where C is the concentration of natrin, IC_{50} is a half-inhibiting concentration value ($IC_{50} = 34.4$ nM), $Block_{max} = 0.69$, and n is the Hill coefficient (1.02). Values of $(I_{control} - I_{natrin})/I_{control}$ were averaged over 3−10 cells.

Concentration Dependence of the Natrin Inhibiting Effect. To determine the dose dependence property of natrin on BK_{Ca} currents, we measured BK_{Ca} currents at a membrane potential of 60 mV following the evocation of a depolarizing pulse using a concentration gradient from 1 nM to 1 μM narin in the bath. The plot of the natrin blocking percentage against the concentrations (Figure 3) showed the inhibition of the BK_{Ca} current by the natrin toxin was concentration-dependent. The current traces were tested on vascular smooth muscle cells held at −60 mV, and the concentration−response curve could be fitted well using a logistic equation. IC_{50} was calculated to be 34.4 nM; the Hill coefficient was 1.02, and the estimated maximal block ratio to the BK_{Ca} currents ($Block_{max}$) was 0.69. In this fit, the squared coefficient of multiple correlation (R^2) was 0.9859, and the adjusted R^2 was 0.9829.

Table 1: Refinement Statistics

resolution range (Å)	8−2.4
no. of reflections[a]	32156
completeness[b] (%)	98.1 (95.0)
R_{factor} [c] (%)	20.6 (24.0)
R_{free} [d] (%)	23.5 (28.0)
no. of protein/solvent atoms	5084/426
mean B-factor for protein (Å^2)	40.30
rmsd for bond distances (Å)	0.006
rmsd for bond angles (deg)	1.2

[a] Observed reflections ($|F_{obs}|/\delta|F_{obs}| > 2.0$) were used for refinement. [b] Values in parentheses correspond to the last resolution shell from 2.40 to 2.51 Å. [c] R-factor $= \sum_j||F_{obs}(j)| - |F_{cal}(j)||/\sum_j|F_{obs}(j)|$, where F_{obs} and F_{cal} are the observed and calculated structure factors for reflection j, respectively. [d] The free R-factor was calculated using 5% of the recorded data which were omitted from refinement.

Solution Structure and Quality of the Model. By molecular replacement, the trimer model of natrin in an asymmetric unit has been determined, despite it being present as a monomer in solution (data not shown). The final model has a crystallographic R-factor of 20.6% and a free R-factor of 23.5% (Table 1). The model has good stereochemistry; 89.4% of the main chain torsion angles lie within the most

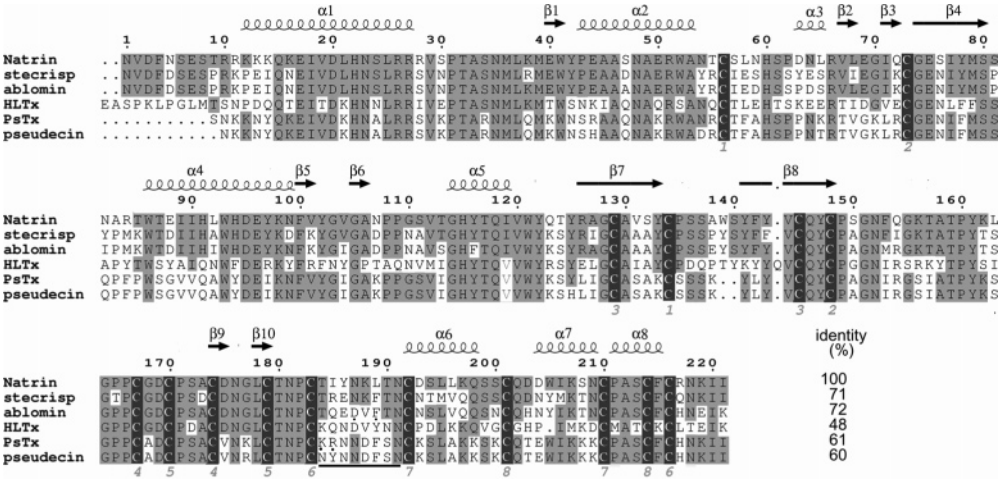

FIGURE 4: Sequence alignment of ion channel blockers in the CRISP family: ablomin (L-Ca^{2+} channel), HLTx (Kv channels), PsTx (CNG channels), and pseudecin (CNG channels). Gene accession codes are given: AAP85301 for natrin, AAQ98964 for stecrisp, Q8JI40 for ablomin, U13619 for HLTx, AY072695 for PsTx, and AY072696 for pseudecin. The indication at the top of the alignment is the DSSP assigned secondary structure of natrin: helix (α1−α8), residues 12−28, 43−53, 63−66, 87−98, 114−119, 192−198, 204−210, and 212−216; *β*-sheet (*β*1−*β*10), residues 40 and 41, 67 and 68, 71 and 72, 74−80, 100 and 101, 105 and 106, 126−132, 141−148, 175 and 176, and 178 and 179. The residues identical to ablomin are shaded. Gaps (−) have been inserted to maximize the level of identity. All cysteine residues are shown in reversed character. Digits under each column indicate eight disulfide bridges in the natrin structure [(1) Cys56−Cys134, (2) Cys73−Cys148, (3) Cys129−Cys145, (4) Cys167−Cys174, (5) Cys170−Cys179, (6) Cys183−Cys216, (7) Cys192−Cys210, and (8) Cys201−Cys214]. Numbers at the end of each sequence are level of identity (%) vs natrin. The potentially functional residues are denoted with dots, which have been suggested in previous studies. A segment of residues 184−191 indicated by a thick line is highly variable in these proteins.

favored regions of the Ramachandran plot, with a further 15.1% in the generously allowed regions and no residues in the disallowed regions (*29*).

The final $2F_o - F_c$ electron density map shows good density for almost all of the polypeptide chains. In the final model, there are 644 amino acid residues that belong to three molecules, A (residues 6−221), B (residues 6−221), and C (residues 10−221), two ethanol molecules, and 424 water molecules in the asymmetric unit. There was no interpretable density for residues 1−5 of molecules A and B or residues 1−9 of molecule C. Furthermore, densities of side chains of some surface residues are also not discernible: Gln154 and Lys197 (molecule A), Lys13, Gln154, and Lys156 (molecule B), and Lys13, Asn82, Gln154, and Lys156 (molecule C). Most of them are located in flexible loop regions. Consistently, thermal motion factors of these residues in loops (81−85, 107−109, 135−139, and 152−155) are relatively high, and great deviations are observed in these loops (81−85, 107−109, and 135−139) when the Cα atoms of the N-terminal domain in the three molecules are superimposed.

Overall Crystallographic Structure. The overall structure of natrin resembles that of stecrisp with two structurally separate domains, the N-terminal α/*β*/α-sandwich motif (PR-1 domain) (residues 1−160) and the C-terminal cysteine-rich domain (CRD) (residues 183−221) linked by a compact hinge region (residues 161−182). The same disulfide bridges formed by the 16 characteristic cysteines are also present in natrin, with three in the PR-1 domain, three in CRD, and two in the hinge region, as well as those in stecrisp (Figure 4). This three-region architecture of natrin is stabilized by hydrogen bonding interactions between the PR-1 domain (residues 32−36) and the hinge, together with the hydrophobic packing interactions formed by residues T180 and P182 (in the hinge region), L37, I71, Y122, and P149 (in the PR-1 domain), and Y186, I220, and I221 (in CRD, Figure 5C).

In the crystallographic trimer model, the PR-1 domain of one molecule is packing against the CRD of the adjacent molecule by both hydrogen bonding and hydrophobic interactions (Figure 5A). There is not a strict 3-fold symmetry in the trimer, mainly due to the different conformation of molecule C. Molecules A and B are similar, and the rms deviation (rmsd) in the superimposed 216 Cα positions is 0.36 Å. However, molecule C is quite distinct, with a rmsd of 0.67 Å in 212 Cα positions aligned with molecule A and a rmsd of 0.88 Å in 212 Cα positions aligned with molecule B. As shown in Figure 5B, these differences apparently arise from the change in the relative orientation of the PR-1 domain and CRD. Protein Domain Motion Analysis (DynDom) provides an automatic procedure for analyzing protein conformational changes and can detail the relative motion between the two domains (*32*). The result of the analysis showed that the rotation angles are 7.4° between molecules A and C and 9.4° between molecules B and C (Figure 5B). The program also determines that the motion of two domains is attributed to a change in some dihedral angles in the hinge: ΔΨ between residues 182 and 183 is 13.5°, and ΔΨ between residues 183 and 184 is 11.4° (A/C); ΔΨ between residues 182 and 183 is 15.1°, and ΔΨ between residues 183 and 184 is 18.6° (B/C).

Analysis of the interdomain interface indicates that the relative rotation should be constrained by the weak hydrophobic interactions at the interface of two domains (as mentioned above), some long-range hydrogen bonds between Y186 and Y125, Y186, and Q123, and the spatial hindrance between T190 and F153 (Figure 5C).

Comparison with the Crystal Structure of Stecrisp. Superposition of the overall crystallographic structures of natrin and stecrisp shows that the aligned rmsd is 1.3 Å. The major

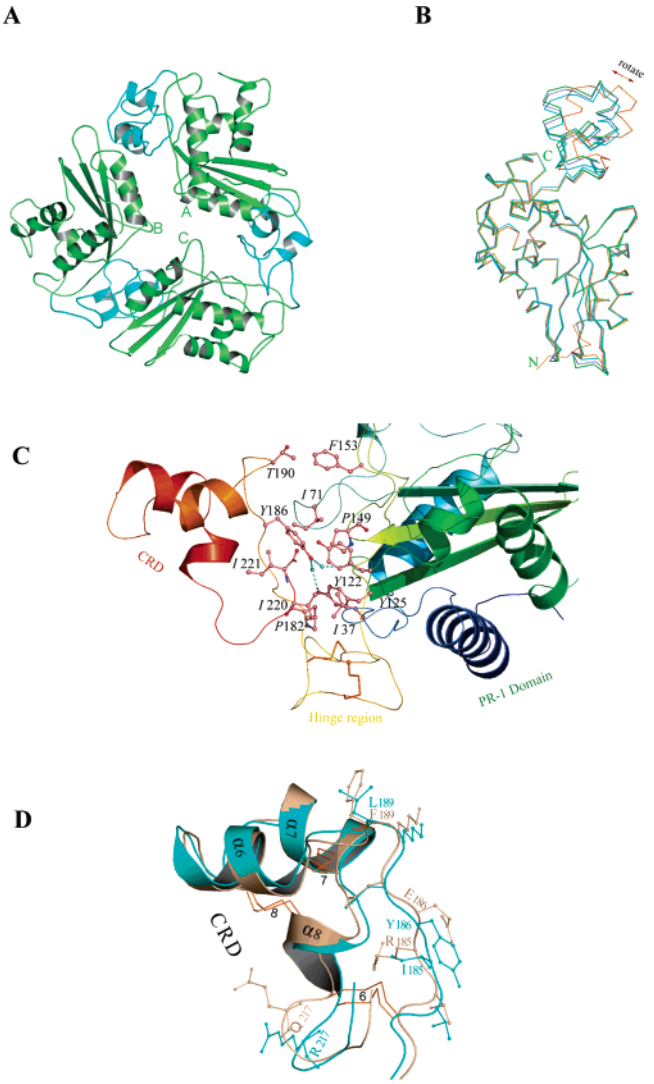

FIGURE 5: Structural analysis of natrin. (A) The trimer model of natrin (PDB entry 1XX5) is indicated, each molecule of which is composed of two domains: PR-1 domain (green) and CRD (cyan). (B) The models were superimposed with the secondary structure of the PR-1 domain using O. Molecules A−C of natrin and stecrisp are colored blue, green, cyan, and orange, respectively. They display a rotation of CRD around the PR-1 domain. Loops of residues 81−85, 107−109, and 135−139 are flexible and show apparent deviations. (C) The hydrophobic interactions stabilize the linkage of CRD (red) and the PR-1 domain (blue) in natrin. The highlighted residues include Leu37, Ile71, Tyr122, and Pro149 in the PR-1 domain and Pro182, Try186, Ile220, and Ile221 in CRD. Two disulfide bridges sustaining the hinge region are colored orange. In addition, there are long-range hydrogen bonds between Tyr186 and Tyr125 and between Tyr186 and Gln123 mediated with two water molecules shown as cyan spheres, and the spatial hindrance between T190 and F153 at this interface. (D) The CRD in molecule A of natrin (cyan) is superimposed with the CRD of stecrisp (wheat, PDB entry 1RC9). The six cysteine residues form three disulfide bonds (orange in CRD; numbers 6−8 indicating disulfide bridges). The potential functional loop (residues 184−189) and residue 217 are depicted in stick representation and labeled in natrin and stecrisp. All figures were prepared with PyMOL (www.pymol.org).

difference is induced by the change of the relative orientation of two domains, which is similar to the conformational change observed in the natrin trimer. The angle deviation of these two domains between natrin and stecrisp is 16.7° (Figure 5B). When they are superposed with the individual domains, the aligned rmsd's are 0.27 Å in the hinge region, 0.5 Å in the PR-1 domain, and 1.2 Å in CRD. There is no obvious deviation in the hinge region consisting of the highly conservative residues. In the PR-1 domain, the prominent deviation is mainly located in the flexible loops. In CRD, it is apparent that a large deviation exists in two solvent-exposed loops: (i) a long loop comprised of residues 183−191 (loop I) and (ii) a small loop of residues 217−221 (loop III) (Figure 5D). The long loop consists of significantly variable residues and participates in the interface between the PR-1 domain and CRD only by weak interactions. As a result, this loop is flexible in undergoing conformational change for deduction of the interdomain motion as described before. After the CRD of natrin is superimposed on that of stecrisp, the deviation in CA atoms is 2.0, 1.5, and 1.0 Å in the three variable residues (R185I, E186Y, and F189L, respectively) in loop I (Figure 5D). In addition to the long loop, a short loop (loop III) with relatively conservative residues is also found to undergo a conformational change, especially for residue 217. Lys217 of natrin has the opposite charge of Glu217 of stecrisp and flips out directly, inducing a different orientation of this side chain. The conformational change in loop I is restrained by loop III by hydrogen bonding and a disulfide bonding interaction between both loops.

DISCUSSION

A Novel BK_{Ca} Channel Blocker. Recently, some proteins of CRISPs in the snake venom have been found to act on L-type Ca^{2+} channels or CNG channels. But so far, snake toxins in CRISPs have still not been reported to interact with K^+ channels. Here, natrin purified from *N. atra* venom, as a member of the CRISP family, was first shown to block BK_{Ca} channels in CRISPs. In the isolated vessel of mouse, 1 μM natrin could induce a further contractile tone in the denuded thoracic aorta, which was contracted with 60 mM K^+ solution before or after, without affecting basal tension (Figure 1). These results are different from the study of other proteins of CRISPs in snake venoms: ablomin, trifling, and latisemin which can block vascular smooth muscle contraction induced by a 60 mM K^+ solution maybe by inhibiting L-type Ca^{2+} channels (*19*). As we know, a 60 mM K^+ solution can alter K^+ equilibrium potential to induce depolarization which activates voltage-gated Ca^{2+} channels and causes an increase in the $[Ca^{2+}]_i$ in VSMCs (*33*). If the drug can block voltage-gated Ca^{2+} channels, vascular smooth muscle contraction induced by a 60 mM K^+ solution will be potential. Because of this relationship, the probable effect of natrin to inhibit voltage-gated Ca^{2+} channel can be eliminated. On the other hand, the increase in $[Ca^{2+}]_i$ can activate BK_{Ca} channels sharply to repolarize, reducing $[Ca^{2+}]_i$ (*34*). When the drug can block BK_{Ca} channels, this repolarization induced by BK_{Ca} channels will be canceled and $[Ca^{2+}]_i$ in VSMCs will sequentially increase, inducing a further contractile response in the vessel. In the membrane of VSMCs, three types of K_{Ca} channels (BK_{Ca}, IK_{Ca}, and SK_{Ca}) are coexistent and all sensitive to an increase in $[Ca^{2+}]_i$, but only the BK_{Ca} channel is also sensitive to voltage and is expressed abundantly in VSMCs. So, we used whole-cell voltage clamp to activate BK_{Ca} currents on a single VSMC and found natrin could block BK_{Ca} currents with high affinity (IC_{50} = 34.4 nM). This finding has also further explained natrin-induced contraction of isolated vessels in a 60 mM K^+ solution.

However, at the rest state of the membrane potential of VSMCs, BK_{Ca} channels which are almost not open hardly contribute to rest membrane potential. Thus, natrin could not affect the basal tension of the denuded thoracic aorta. As a blocker of BK_{Ca} channels of VSMCs, natrin may induce hypertension when it is injected into a person's blood, which probably is related to some cardiovascular sickness.

In concentration−response experiments, the curve was fitted by using a Hill coefficient *n* of 1.02, suggesting that only a single natrin molecule must bind to a BK_{Ca} channel to block its current. It is consistent with its biological unit as the monomer in solution (data not shown), though there is a trimer in an asymmetric unit of its crystal. Similar results which show that PsTx toxin can interact with CNG channels in the molar ratio of 1:1 have been reported (*17*). With the apparently high molecular mass relative to those of most known peptide blockers, CRISPs are likely to compose a distinct class of ion channel blockers.

Though natrin's effect on BK_{Ca} channels has been well proven, whether natrin can affect some other kinds of ion channels is still unclear. In previous studies, some proteins of CRISPs in the snake venom, e.g., HLTx and ablomin, can act on different ion channels (*21*, *22*, *35*). Therefore, subsequent studies of natrin will be emphasized on other targets.

Domain Motion in Natrin. We determined the structure of natrin and further analyzed the structural relationship of the two domains. The results show the packing interface of two domains is too weak to restrain completely the relative position of two domains. It is clear that CRD can rotate around the PR-1 domain by the change of some dihedral angles in the hinge (residues 182−184) in the trimer model. But this behavior cannot be observed in the crystal of setcrisp because there is only one molecule in an asymmetric unit. A great deal of data of interdomain's motion described before came from X-ray structures of particular proteins under different conditions, e.g., environmental change (varying pH and temperature levels), and binding interactions between proteins, nucleic acids, ligands, and small molecules. However, this motion can be observed under the same conditions in the natrin crystal. It is well-known that the interdomain motion plays an important role in a variety of biological phenomena such as catalysis, transport, formation of large assemblies, and cellular locomotion (*36*, *37*). It has been reported that this motion in the solution only spends a small amount of energy (*38*). This interdomain motion in the natrin crystal structure implies that this CRD may be relatively flexible in the solvent and serve as an independent protein−protein interaction module.

Potential Functional Residues in CRD. According to previous studies of PsTx and pseudecin that can block CNG channels with different affinity, two adjacent critical residues (Lys174 and Arg175) in PsTx were suggested to interact with CNG channels (*18*, *35*). Other studies of ablomin, triflin, latismin, Glu186, and Phe189 were thought to be potential functional residues contributing to the inhibition of smooth muscle contraction likely by blocking L-type Ca^{2+} channels (*19*, *35*, *39*). On the basis of structural models of natrin and stecrisp, these critically functional residues lie in exposed solvent loop I of CRD, which can participate in a smooth interface in which the side chains do not interdigitate. As determined by alignment, this loop is hypervariable in their primary sequence among these highly homologous CRISPs and undergoes conformational change for these variable residues between the superposed structures of the CRD in natrin and stecrisp, which suggests that there may be different extents of deviation in loop I in these proteins (Figures 4 and 5D). Interestingly, this loop of a molecule interacts with other packing molecules in both natrin and strecrisp crystal, which further shows this loop easily interacts with other proteins. Thus, the deviation and variable residues in loop I may contribute to different effects of some proteins of CRISPs on protein−protein interaction, although other regions may also provide additional interactions. By structural alignment with ShK and BgK K^+ channel blocker toxins from sea anemone, this CRD of natrin also displays a striking homology with them, as well as that of stecrisp described previously (*22*). According to some binding studies of ShK and BgK, a functional dyad including a positive residue and a hydrophobic residue of the aromatic ring can interact with K^+ channels. Furthermore, the dyads of both toxins lying in the same helix display a similar spatial organization of the side chains (*23*). Though the CRD of natrin shares a similar folding pattern with BgK and ShK toxins, the dyad has been variable in the appropriate position of the CRD of natrin. This implies it may participate in another interaction with channels, differing from the ShK and BgK channels. However, at present, we still lack the direct evidence for the role of the CRD of natrin in interacting with BK_{Ca} channels. Identification of the binding site in natrin needs further investigation.

ACKNOWLEDGMENT

We thank the Information Science Center of the University of Science and Technology of China for providing the SGI workstation and Dr. J. Navazza for providing AMoRe, Dr. A. T. Brünger for providing CNS, Dr. T. A. Jones for providing O, and Dr. Warren L. DeLano for providing PyMol.

SUPPORTING INFORMATION AVAILABLE

Homogeneity, molecular weight, and biological unit in solution of natrin demonstrated by SDS−PAGE, mass spectrometry, and size exclusion chromatography and interaction between the two molecules of the trimer in the natrin crystal. This material is available free of charge via the Internet at http://pubs.acs.org.

REFERENCES

1. Nelson, M. T., and Quayle, J. M. (1995) Physiological roles and properties of potassium channels in arterial smooth muscle, *Am. J. Physiol. 268*, 799−822.
2. Weiger, T. M., Hermann, A. L., and Evitan, I. B. (2002) Modulation of calcium-activated potassium channels, *J. Comp. Physiol., A 188*, 79−87.
3. Jackson, W. F. (2000) Ion channels and vascular tone, *Hypertension 35*, 173−178.
4. Gregory, J. K., Hans-Gunther, K., Reid, J. L., Owen, B. M., and Maria, L. G. (1996) High-conductance calcium-activated potassium channels; structure, pharmacology, and function, *J. Bioenerg. Biomembr. 28*, 255−267.
5. Knot, H. J., and Nelson, M. T. (1998) Regulation of arterial diameter and wall [Ca^{2+}] in cerebral arteries of rat by membrane potential and intravascular pressure, *J. Physiol. 508*, 199−209.

6. Jaggar, J. H., Porter, V. A., Lederer, W. J., and Nelson, M. T. (2000) Calcium sparks in smooth muscle, *Am. J. Physiol. 278*, C235−C256.
7. Jaggar, J. H., Wellman, G. C., Heppner, T. J., Porter, V. A., Perez, G. J., Gollasch, M., Kleppisch, T., Rubart, M., Stevenson, A. S., Lederer, W. J., Knot, H. J., Bonev, A. D., and Nelson, M. T. (1998) Ca^{2+} channels, ryanodine receptors and Ca^{2+}-activated K^+ channels: A functional unit for regulating arterial tone, *Acta Physiol. Scand. 164*, 577−587.
8. Shieh, C.-C., Coghlan, M., Sullivan, J. P., and Gopalakrishnan, M. (2000) Potassium channels: Molecular defects, diseases, and therapeutic opportunities, *Pharmacol. Rev. 52*, 557−593.
9. Butler, A., Tsunoda, S., McCobb, D. P., Wei, A., and Salkoff, L. (1993) mSlo, a complex mouse gene encoding "maxi" calcium-activated potassium channels, *Science 261*, 221−224.
10. Doyle, D. A., Cabral, J. M., Pfuetzner, R. A., Kuo, A. L., Gulbis, J. M., Cohen, S. L., Chait, B. T., and MacKinnon, R. (1998) The structure of the potassium channel: Molecular basic of K^+ conduction and selectivity, *Science 280*, 69−77.
11. Jiang, Y. X., Lee, A., Chen, J. Y., Ruta, V., Cadene, M., Chait, B. T., and Mackinnon, R. (2003) X-ray structure of a voltage-dependent K^+ channel, *Nature 423*, 33−41.
12. Gimenez, G., Navia, M. A., Reuben, J. P., Katz, G. M., Kaczorowski, G. J., and Garcia, M. L. (1988) Purification, sequence, and model structure of charybdotoxin, a potent selective inhibitor of calcium-activated potassium channels, *Proc. Natl. Acad. Sci. U.S.A. 85*, 3329−3333.
13. Stampe, P., Kolmakova-Partensky, L., and Miller, C. (1994) Intimations of K^+ channel structure from a complete functional map of the molecular surface of charybdotoxin, *Biochemistry 33*, 443−450.
14. Crest, M., Jacquet, G., Gola, M., Zerrouk, H., Benslimane, A., Rochat, H., Mansuelle, P., and Martin-Eauclaire, M. F. (1992) Kaliotoxin, a novel peptidyl inhibitor of neuronal BK-type Ca^{2+}-activated K^+ channels characterized from *Androctonus mauretanicus mauretanicus* venom, *J. Biol. Chem. 267*, 1640−1647.
15. Cai, Z., Xu, C. Q., Xu, Y. Q., Lu, W. Y., Chi, C. W., Shi, Y. Y., and Wu, J. H. (2004) Solution structure of BmBKTx1, a new BK_{Ca} channel blocker from the chinese scorpion *Buthus martensi* Karsch, *Biochemistry 43*, 3764−3771.
16. Wang, J., Guo, M., Tu, X. Y., Zheng, D. H., Teng, M. K., Niu, L. W., Liu, Q., Huang, Q. Q., and Hao, Q. (2004) Purification, partial characterization, crystallization and preliminary X-ray diffraction of two cysteine-rich secretory proteins from *Naja atra* and *Trimeresurus stejnegeri venoms*, *Acta Crystallogr. D60*, 1108−1111.
17. Brown, R. L., Haley, T. L., West, K. A., and Crabb, J. W. (1999) Pseudechetoxin: A peptide blocker of cyclic nucleotide-gated ion channels, *Proc. Natl. Acad. Sci. U.S.A. 96*, 754−759.
18. Yamazaki, Y., Brown, R. L., and Morita, T. (2002) Purification and cloning of toxins from elapid venoms that target cyclic nucleotide-gated ion channels, *Biochemistry 41*, 11331−11337.
19. Yamazaki, Y., Koike, H., Sugiyama, Y., Motoyoshi, K., Wada, T., Hishinuma, S., Mita, M., and Morita, T. (2002) Cloning and characterization of novel snake venom proteins that block smooth muscle contraction, *Eur. J. Biochem. 269*, 2708−2715.
20. Morrissette, J., Krätzschmar, J., Haendler, B., El-Hayek, R., Mochca-Morales, J., Martin, B. M., Patel, J. R., Moss, R. L., Schleuning, W. D., Coronado, R., and Possani, L. D. (1995) Primary structure and properties of helothermine, a peptide toxin that blocks ryanodine receptors, *Biophys. J. 68*, 2280−2288.
21. Nobile, M., Magnelli, V., Lagostena, L., Mochca-Morales, J., Possani, L. D., and Prestipino, G. (1994) The toxin helothermine affects potassium currents in newborn rat cerebellar granule cell, *J. Membr. Biol. 139*, 49−55.
22. Guo, M., Teng, M. K., Niu, L. W., Liu, Q., Huang, Q. Q., and Hao, Q. (2005) Crystal structure of cysteine-rich secretory protein stecrisp reveals the cysteine-rich domain has a K^+-channel inhibitor-like fold, *J. Biol. Chem. 280*, 12405−12412.
23. Dauplais, M., Lecoq, A., Song, J., Cotton, J., Jamin, N., Gilquin, B., Roumestand, C., Vita, C., De Medeiros, C. L. C., Rowan, E. G., Harvey, A. L., and Ménez, A. (1997) On the convergent evolution of animal toxins: Conservation of a dyad of functional residues in potassium channel-blocking toxins with unrelated structures, *J. Biol. Chem. 272*, 4302−4309.
24. Tudor, J. E., Pallaghy, P. K., Pennington, M. W., and Norton, R. S. (1996) Solution structure of ShK toxin, a novel potassium channel inhibitor from a sea anemone, *Nat. Struct. Biol. 3*, 317−320.
25. Ye, C. L., Shen, B., Ren, X. D., Luo, R. J., Ding, S. Y., Yan, F. M., and Jiang, J. H. (2004) An increase in opening of BKCa channels in smooth muscle cells in streptozotocin induced diabetic mice, *Acta Pharmacol. Sin. 25*, 744−750.
26. Navazza, J. (1994) AMoRe: An automated package for molecular replacement, *Acta Crystallogr. B50*, 157−163.
27. Brunger, A. T., Adams, P. D., Clore, G. M., Delano, W. L., Gros, P., Grosse-Kunstleve, R. W., et al. (1998) Crystallography & NMR system: A new software suite for macromolecular structure determination, *Acta Crystallogr. D54*, 905−921.
28. Jones, T. A., Zou, J. Y., Cowan, S. W., and Kleldgaard, M. (1991) Improved methods for building protein models in electron density maps and the location of errors in these models, *Acta Crystallogr. A47*, 110−119.
29. Laskowski, R. A., MacArthur, M. V., Moss, D. S., and Thornton, J. M. (1993) PROCHECK: A program to check the stereochemical quality of protein structure, *J. Appl. Crystallogr. 26*, 283−291.
30. Kim, N., Chung, J., Kim, E., and Han, J. (2003) Changes in the Ca^{2+}-activated K^+ channels of the coronary artery during left ventricular hypertrophy, *Circ. Res. 93*, 541−547.
31. Bae, Y. M., Park, M. K., Lee, S. H., Ho, W. K., and Earm, Y. E. (1999) Contribution of Ca^{2+}-activated K^+ channels and non-selective cation channels to membrane potential of pulmonary arterial smooth muscle cells of the rabbit, *J. Physiol. 514*, 747−758.
32. Hayward, S., and Berendsen, H. J. C. (1998) Systematic analysis of domain motions in proteins from conformational change, new results on citrate synthase and T4 lysozyme, *Proteins 30*, 144−154.
33. Chen, X. L., and Rembold, C. M. (1995) Phenylephrine contracts rat tail artery by one electromechanical and three pharmacomechanical mechanisms, *Am. J. Physiol. 268*, H74−H81.
34. Brayden, J. E., and Nelson, M. T. (1992) Regulation of arterial tone by activation of calcium-dependent potassium channels, *Science 256*, 532−535.
35. Yamazaki, Y., and Morita, T. (2004) Structure and function of snake venom cysteine-rich secretory proteins, *Toxicon 44*, 227−231.
36. Yon, J. M., Perahia, D., and Ghelis, C. (1998) Conformation dynamics and enzyme activity, *Biochimie 80*, 33−42.
37. Gerstein, M., and Krebs, W. (1998) A database of macromolecular motions, *Nucleic Acids Res. 26*, 4280−4290.
38. Gerstein, M., Lesk, A. M., and Chothia, C. (1994) Structural mechanisms for domain movements in proteins, *Biochemistry 33*, 6739−6749.
39. Yamazaki, Y., Hyodo, F., and Morita, T. (2003) Wide distribution of cysteine-rich secretory proteins in snake venoms: Isolation and cloning of novel snake venom cysteine-rich secretory proteins, *Arch. Biochem. Biophys. 412*, 133−141.

BI050614M